Journal of Alloys and Compounds 509 (2011) 10092–10097

Contents lists available at ScienceDirect

Journal of Alloys and Compounds

journal homepage: www.elsevier.com/locate/jallcom

Chemical route to synthesis of mesoporous ZnO thin films and their liquefied petroleum gas sensor performance

D.S. Dhawale, C.D. Lokhande*

Thin Film Physics Laboratory, Department of Physics, Shivaji University, Kolhapur- 416 004 (M. S.) India

ARTICLE INFO

Article history:
Received 24 May 2011
Received in revised form 9 August 2011
Accepted 9 August 2011
Available online 16 August 2011

Keywords:
ZnO
Thin films
Mesoporous
CBD
LPG sensor

ABSTRACT

In the present work, we report base free chemical bath deposition (CBD) of mesoporous zinc oxide (ZnO) thin films from urea containing bath for liquefied petroleum gas (LPG) sensor application. Mesoporous morphology with average pore size ~2 μm and wurtzite crystal structure are confirmed from scanning electron microscopy (SEM) and X-ray diffraction (XRD) analysis. The surface of ZnO is hydrophobic with water contact angle 128 ± 1°. Optical study reveals the presence of direct bad gap with energy 3.24 eV. The gas sensing study reveals the mesoporous ZnO is highly selective towards LPG as compared with CO_2 and maximum LPG response of 52% is achieved upon the exposure of 3900 ppm LPG at 573 K as well as good reproducibility and short response/recovery times.

1. Introduction

Liquefied petroleum gas (LPG) is potentially hazardous because explosion accidents might be caused when it leaks out by mistake. So, there is a great demand from the society of detecting LPG for the purpose of safety applications in domestic and industrial fields. In the past decades, solid-state gas sensors have played an important role in environment monitoring and chemical process controlling. Among the various solid-state sensors, semiconducting metal oxide sensors have been widely investigated due to their small dimensions, low cost and high compatibility with Si-based microelectronics. Metal oxide gas sensors are widely used in industry, environmental monitoring and medical diagnosis, for the detection of a variety of toxic and flammable gases. One of the most promising approaches for the realization of high performance gas sensors is the development of nanostructured metal oxide sensing materials [1]. Till now, a number of efficient gas sensors based on semiconducting nanostructured metal oxides such as SnO_2 [1], TiO_2 [2], ZnO [3], CdO [4] and NiO [5], have been successfully synthesized. Among them, nanostructured ZnO is one of the most studied n-type semiconducting oxide material with a wide direct band gap (~3.3 eV) and high exciton binding energy (60 meV), since it has been widely utilized in the fields of transparent conducting electrodes, varistors, gas sensors and optoelectronic devices [6]. Recently, nanostructured ZnO as an II–VI compound semiconductor has been proven to be an excellent gas sensitive material for detection of LPG [7] ethanol [8], NO_2 and acetone [9], H_2 [10] as well as for photoconductive UV sensor [11].

Up to now, various methods have been reported for the preparation of different ZnO nanostructures such as nanowires [12], nanorods [7], flower-like [13,14], rhombus-shaped [15], interconnected network-like [16], etc. In contrast with some other nanostructures, the hierarchically porous nanostructures can provide novel pattern for exploring unique properties and superior device performances. The conventional methods for preparing porous or hollow materials usually require the use of pore directing reagents or templates and may suffer from contamination due to the uncompleted removal of the additives either by chemical etching or thermal treatment [17,18]. Therefore, to develop facile, economical, template-free synthetic strategies to synthesize porous materials is of great significance from the view of both scientific research and practical applications. Although it has been often claimed that the growth of porous nanostructures can be performed with low-cost technologies, the high complexity in nanostructure-based device realization often makes them sensibly more costly than sensors produced by simple synthesis techniques as, for example, chemical bath deposition (CBD) method. As one of the solution chemical route, CBD method [7] becomes a promising option for large-scale production, which is simpler, faster and less expensive. Control of morphology is currently a key issue in developing functional materials and much effort has been undertaken for upgrading the characteristics of materials [19]. However, earlier works focused on stabilizing specific forms rather than providing a strategy to freely direct the porous morphology [7,20]. Direct

* Corresponding author. Tel.: +91 231 2609229; fax: +91 231 2692333.
E-mail address: l.chandrakant@yahoo.com (C.D. Lokhande).

0925-8388/$ – see front matter © 2011 Elsevier B.V. All rights reserved.
doi:10.1016/j.jallcom.2011.08.046

fabrication of porous materials with fully tunable morphology still remains a challenge. Using solution systems, the morphology control and nano/micro manufacturing of oxide materials is possible. Solution systems have the advantage of adjustment of supersaturation degree and high uniformity in the system for particle morphology control.

Herein, for the first time, we present a one-step, base free, seedless method for the synthesis of mesoporous ZnO thin films onto glass substrates at low temperature through a simple method involving controlled chemical precipitation based on principles of ionic and solubility products for LPG sensor application. Before testing for gas sensor performance, these films were characterized for their structural, morphological, surface wettability and optical properties and results are discussed in this context. Finally, the gas sensing performance for commercially available LPG and CO_2 has been investigated.

2. Experimental details

Unless otherwise noted, AR chemicals were obtained from commercial suppliers and used without further purification. Mesoporous ZnO thin films were grown onto the glass substrates by soft CBD method in aqueous acidic medium at 353 K using 0.05 M zinc sulphate ($ZnSO_4$) as a Zn^{2+} ion source. For the complex formation, 1 M urea (NH_2CONH_2) solution was added with constant stirring for 5 min. and pH adjusted to ~3 using dil. H_2SO_4. At this stage solution was transparent and free from any precipitates. After stirring for 1 h, this homogeneous solution was kept under unstirred condition in bottle containing glass substrates in the bath and bath was heated to 353 K. During the precipitation, heterogeneous reaction occurred and the deposition of mesoporous $Zn(OH)_2$ thin film took place on the substrates. The substrates coated with mesoporous $Zn(OH)_2$ with different film thicknesses were removed with a time interval of 6, 12, 18 and 24 h from the bath, washed with double-distilled water, dried in air and preserved in an airtight container. As-deposited films were specularly reflecting, uniform and well adherent to the substrates. As-deposited $Zn(OH)_2$ films were converted into ZnO after annealing in air at 623 K for 2 h which generally facilitates decrease in dislocations, stresses, inhomogeneities, removal of hydroxide phase and used for further characterizations.

Thickness was computed by weight difference method using sensitive microbalance with relation $t = \Delta M/(\rho \times A)$ where, 't' – thickness of the film, 'A' – area of the film in cm^2, 'ΔM' = $M_1 - M_2$ – mass of the film deposited on the substrate in grams, 'M_1' – mass of the substrate with film, 'M_2' – mass of the substrate without film and 'ρ' – density of the deposited material (ZnO = 5.675 g/cm^3) in bulk form. In order to acquire more accuracy in results, we measured thickness using the films with maximum area. Also film thickness was measured from cross-section SEM. The structural characterization was carried out using a Philips (PW 3710) X-ray diffractometer with CuKα radiation (λ = 1.5406 Å) in 2θ range from 20 to 80°. Surface morphological images were taken using high-resolution scanning electron microscopy (FE-SEM, Model: JSM-6160) at an acceleration voltage higher than 10 kV for which surface was coated with a 10 nm Au layer before taking images. The static contact angle against water was measured using a contact angle meter (Rame-Hart, CA-X, USA) equipped with CCD camera to observe the shape of water drop on the surface of the ZnO film. Droplet was placed at five different positions and averaged value was adopted as the contact angle. For the optical studies, UV–vis absorption spectrum was measured on a Systronic spectrophotometer-119 with quartz glass substrate as a reference in the wavelength range of 350–750 nm.

The gas sensing properties of ZnO was studied in the home-built gas sensor assembly described earlier [3]. For electrical measurements, silver paste contacts (1 mm) were formed on the ZnO sample of area 1 cm × 1 cm. The electrical resistance of ZnO film in air (R_a) and in the presence of LPG (R_g) was measured to evaluate the gas response, S (%), defined as follows,

$$S(\%) = \frac{R_a - R_g}{R_a} \times 100 \quad (1)$$

3. Results and discussion

3.1. Film formation mechanism

In CBD method, film formation observed when the solution is saturated, the ionic product of anion and cation is equal to solubility product of metal oxide and when it exceeds, precipitation occurs and ions combine on the substrate and in the solution to form nuclei. The film growth can take place by ion-by-ion condensation of materials or by adsorption of colloidal particles from the solution on the substrate. The formation of solid phase from a solution involves two steps as nucleation and particle growth. In the present case, we attempted to supply carbon dioxide and ammonium by using a chemical reaction of urea in water. This includes hydrolysis of urea and reaction of ammonium with water as follows,

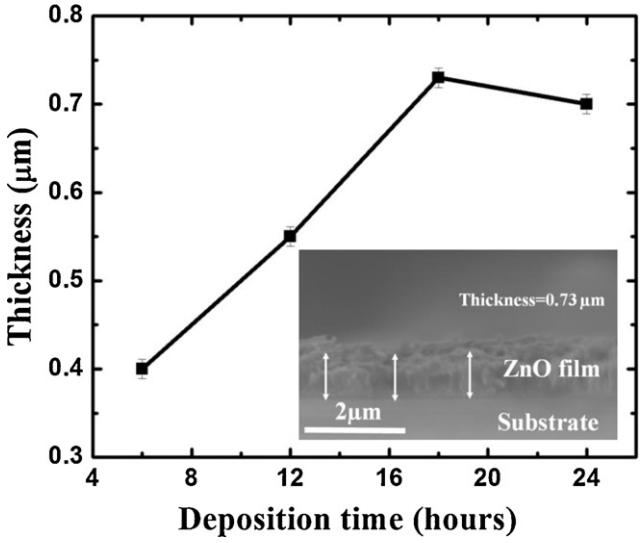

Fig. 1. The variation of ZnO film thickness with deposition time. Inset shows the cross-sectional SEM image of ZnO thin film.

$$NH_2CONH_2 + H_2O \xrightarrow{\Delta 353\,K} CO_2 + 2NH_3 \quad (2)$$

$$NH_3 + H_2O \rightarrow NH_4OH \quad (3)$$

The hydroxide ions (protolytic reaction of ammonia slowly releases the hydroxide ions) and Zn^{2+} cations reacts, to form $Zn(OH)_2$ thin films

$$ZnSO_4 + NH_2CONH_2 + 5H_2O \rightarrow Zn(OH)_2 + 2H_2O + (NH_4)_2SO_4 \quad (4)$$

As-deposited films are transparent, uniform and well adherent to the substrates. After annealing in air at 673 K, as-deposited $Zn(OH)_2$ get converted into ZnO as

$$Zn(OH)_2 \xrightarrow{\Delta 673\,K} ZnO + H_2O \quad (5)$$

Fig. 1 shows the variation of ZnO film thickness with deposition time. Nonlinear rate of increase in the thickness is attributed to the growth by nucleation and coalescence process. This may due to more nucleation sites contribute to coagulation during the growing procedure. The maximum thickness of 0.73 μm is achieved. Film thickness calculated form weight difference method is comparable with measured from cross-sectional SEM image shown in the inset of Fig. 1. Furthermore, slight decrease in thickness is attributed to the formation of outer porous layer and/or the film which may have developed stress which tends to cause delamination, resulting in peeling off the film [21].

3.2. Structural and surface morphological studies

The crystal structure of mesoporous ZnO film is analyzed by XRD pattern shown in Fig. 2. All the peaks of ZnO can be indexed to the wurtzite crystal structure (JCPDS card No.36-1451, a = 3.249 Å, c = 5.206 Å, spacegroup: $P63mc$, no.186). No characteristic peaks of other impurities such as $Zn(OH)_2$ are detected in the diffractogram. Fig. 3(a and b) shows the FESEM images of mesoporous ZnO films at two different magnifications. From the FESEM images, one can conclude that morphology of the ZnO film is highly porous and forms a channel within the grains as seen in low magnification (×10,000). For detail investigation of this morphology, high magnified image (×40,000) is recorded which gives average pore

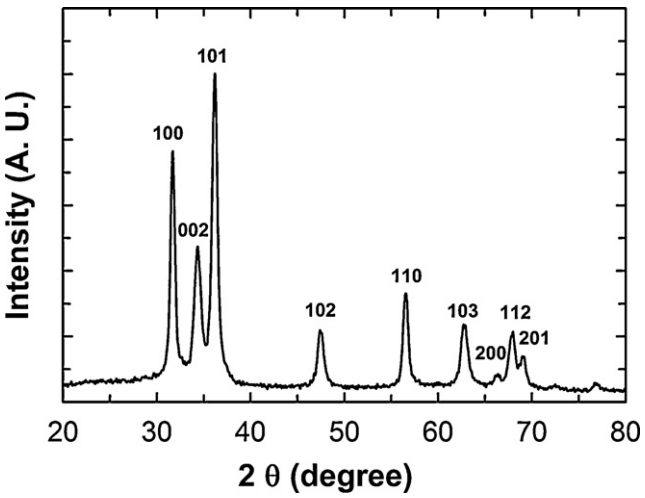

Fig. 2. The X-ray diffraction pattern of mesoporous ZnO thin film.

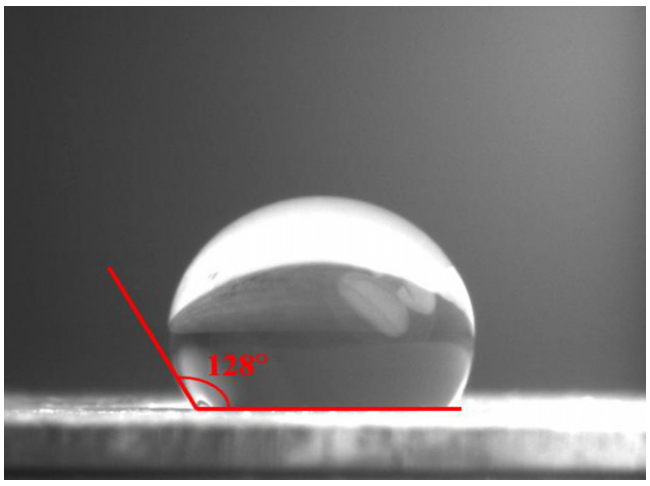

Fig. 4. Photoimage of water contact angle measurement with mesoporous ZnO surface.

size ~2 μm. With this morphology chemically deposited mesoporous ZnO can adsorb atmospheric oxygen very easily and the amount adsorbed depends on the area of exposed surface of the film.

3.3. Surface wettability studies

Wettability involves the interaction between a liquid and solid in contact. Wetting is an important property of a surface and controlled by both the chemical nature and the geometrical structure. According to Thomas Young model, interplay between the surface free energies of the solid–liquid, solid–gas and liquid–gas boundaries determined the static water contact angle. Here, as reported earlier [22], we look at the feasibility of said vicinal surface for gas sensor application. Fig. 4 shows the photo image of shape of water droplet on mesoporous ZnO film surface. Interestingly, ZnO film exhibits hydrophobic behavior with contact angle of $128 \pm 1^{\circ}$ ($\theta > 90^{\circ}$). In the present case, the energy cost is typically too high for the water to follow the patterned surface and as a result the droplet recedes, forming an even larger contact angle compared to the smooth surface. In addition, water drop suspended on top of hydrophobic rough surface with air trapped underneath. The value of water contact angle is less than reported values in the literature [23] for annealed ZnO films. This may due to mesoporous surface morphology, which traps less air in between.

3.4. Optical studies

The optical spectrum of mesoporous ZnO film is studied at room temperature in the range of 350–750 nm wavelength without scattering and reflection taking into account. Fig. 5 shows the variation of absorbance with wavelength and it reveals that, film has low absorption in the visible region, which is a characteristic of ZnO. The fundamental absorption, which corresponds to electron excitation from the valence band to conduction band, can be used to determine the nature and value of the optical band gap energy. The optical band gap energy is determined using following relation,

$$\alpha h\upsilon = A(h\upsilon - E_g)^n \quad (6)$$

where, 'A' is a constant, '$h\upsilon$' is the photon energy, 'E_g' is the band gap energy and n is equal to 1/2 for a direct and 2 for indirect transition. The band gap energy is determined from the plot of $(\alpha h\upsilon)^2$ vs. photon energy ($h\upsilon$) shown in inset of Fig. 5. The intercept of the tangent to the $h\upsilon$ axis gives the direct band gap energy and found to be 3.24 eV which is comparable with reported earlier [23]. Since the sensitivity of the gas sensor is, plausibly, a function of band gap of the material.

3.5. Gas sensing properties

The gas sensing mechanism of ZnO based sensor belongs to the surface-controlled type that is, the resistance change is controlled

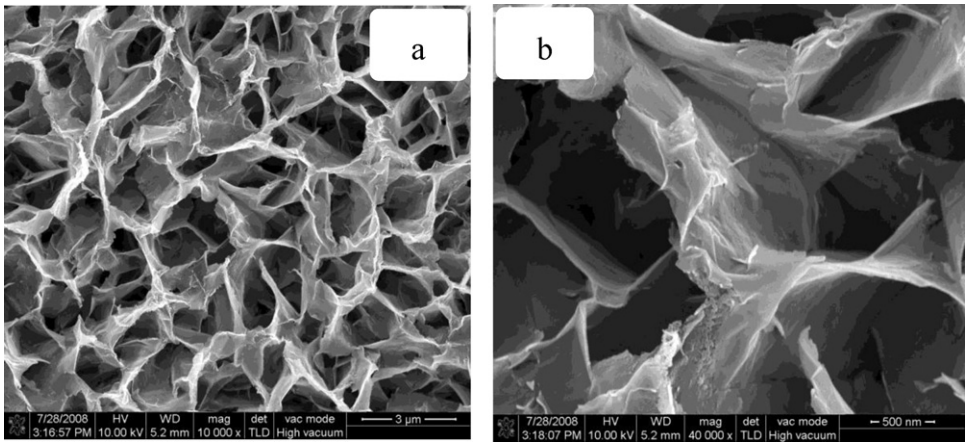

Fig. 3. The FMSEM images of mesoporous ZnO thin film at the magnifications of (a) ×10,000 and (b) ×40,000.

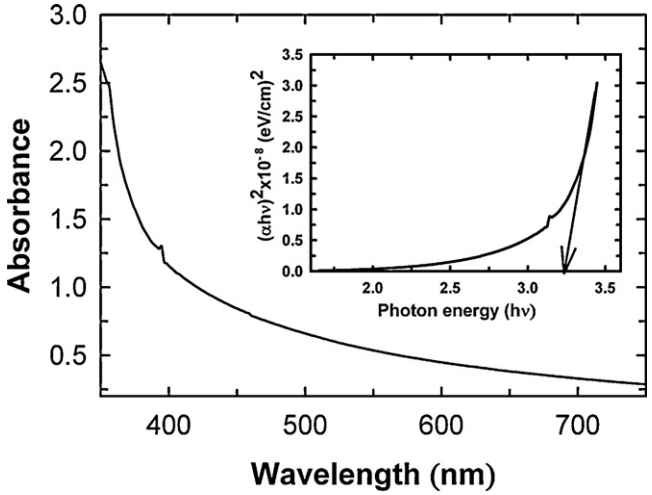

Fig. 5. The variation of absorbance vs. wavelength of mesoporous ZnO thin film. Inset shows variation of $(\alpha h\upsilon)^2$ vs. $h\upsilon$ to determine the direct band gap energy of ZnO film.

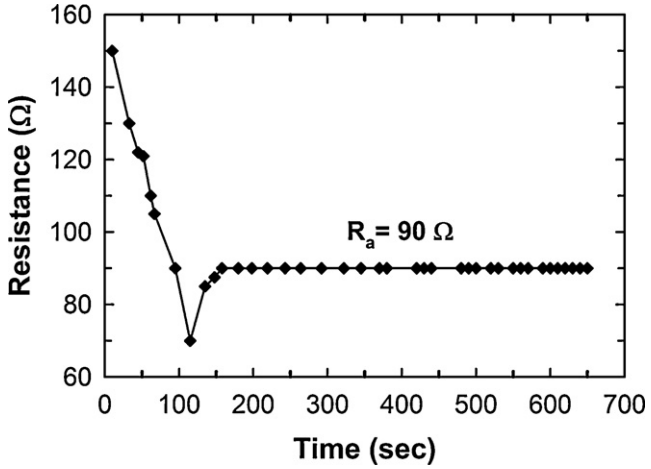

Fig. 6. The stabilization of resistance of mesoporous ZnO at 573 K from non-equilibrium to equilibrium stage.

by the species and amount of chemisorbed oxygen on the surface. At an operating temperature, in the absence of a target gas, oxygen gets adsorbed on the surface of the sensor and it extracts electrons from the conduction band of the sensor material [24] to produce negatively charged chemisorbed oxygens such as O_2^- and O^- which create a depletion layer at the surface of the individual particles and inter-granular regions. As a result, the concentration of electrons in the n-type ZnO decreases and hence the electrical conductance of the material decreases. This process can be expressed by the following [25,26],

$$O_{2(gas)} \leftrightarrow O_{2(adsorbed)} \quad (7)$$

$$O_{2(adsorbed)} + e^- \leftrightarrow O_2{}^-{}_{(adsorbed)} \quad (8)$$

$$O_2{}^-{}_{(adsorbed)} + e^- \leftrightarrow 2O^-{}_{(adsorbed)} \quad (9)$$

When reducing gases are inleted, the interaction of reducing gases with the surface chemisorbed oxygen can take place and thereby releasing electrons back to the conduction band and electrical conductance of the semiconductor increases [27].

3.5.1. Selectivity study

Before the exposure of target gas, the mesoporous ZnO film is allowed to stable for electrical resistance in air and the stabilized resistance taken as R_a. Fig. 6 shows the typical initial stabilization curve of resistance of mesoporous ZnO film in air at 573 K from non-equilibrium to equilibrium. The stabilization of mesoporous ZnO film resistance in ambient air prior to exposure of target gas is important, because it ensures stable zero level for gas sensing applications. Initially, when the temperature of 573 K is attained, the resistance decreased rapidly within few seconds and then raised and exhibited a stable value. Similar type of trend has observed by Dhawale et al. [2] for CBD deposited TiO_2 film. A comparative bar graph of gas responses of mesoporous ZnO sensor is represented in Fig. 7 upon exposure of 2600 ppm concentration towards CO_2 and LPG at 573 K. The mesoporous ZnO sensor exhibits more selective towards LPG as compared to CO_2. The mesoporous ZnO sensor offered maximum response towards CO_2 (17%) and LPG (42%), as different gases have different energies for reaction to occur at the surface of film. Therefore, further gas response is studied for various operating temperatures and LPG concentrations.

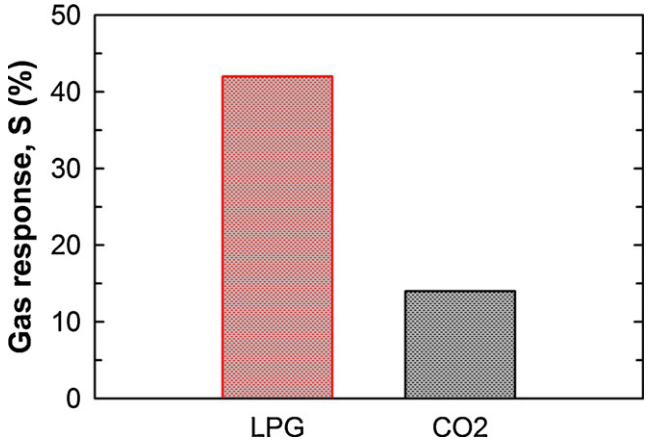

Fig. 7. The comparative gas responses (%) of mesoporous ZnO sensor towards CO_2 and LPG.

3.5.2. Effect of operating temperature

Initially LPG response is studied as a function of operating temperature. Fig. 8 shows the dependence of LPG response of ZnO film

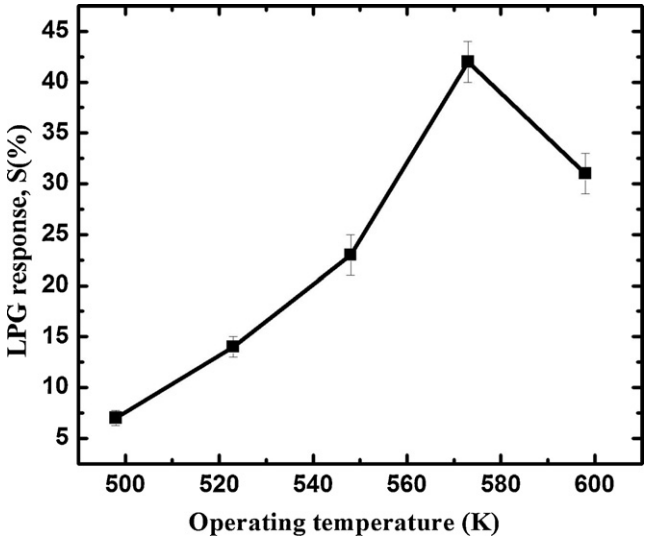

Fig. 8. The variation of an operating temperature with LPG response of mesoporous ZnO sensor at 2600 ppm LPG.

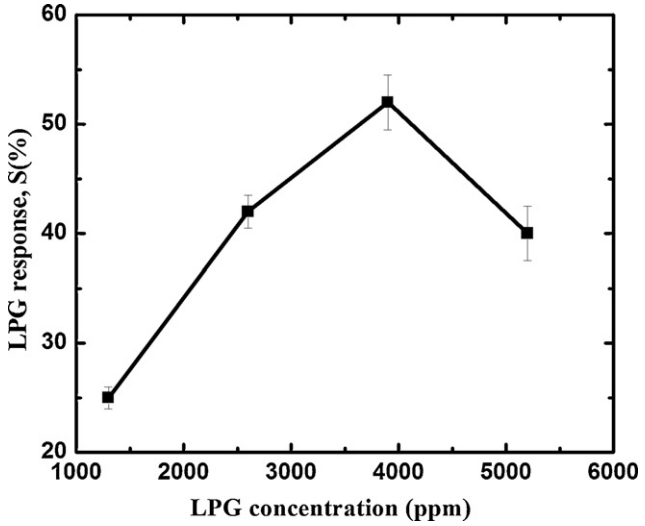

Fig. 9. The variation of LPG response of mesoporous ZnO sensor at 573 K with the different concentration of LPG.

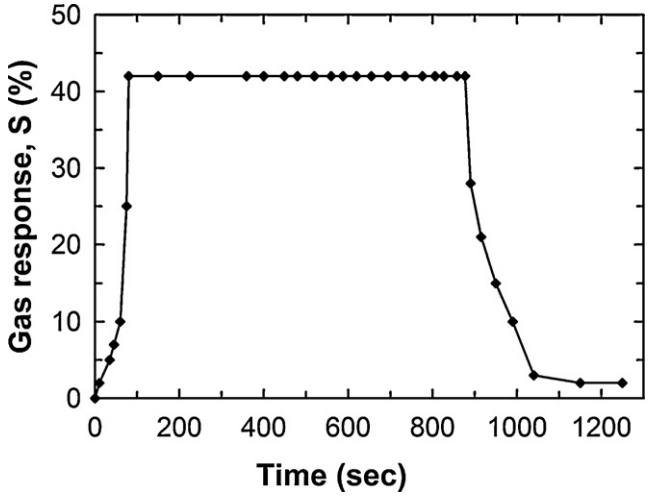

Fig. 10. The response transient of mesoporous ZnO sensor under the exposure of 2600 ppm LPG at 573 K.

towards 2600 ppm LPG which corresponds to 10% of the lower explosive level (LEL) of LPG for different operating temperatures. When the chemically deposited ZnO thin film is heated at a temperature of 498–548 K, the reaction products does not desorbs from the film surface. Nevertheless, they cover the sensing sites on the surface of the film which prevents further reaction of the LPG with chemisorbed oxygen. Subsequently, no appreciable change in the resistance of the film is observed. At 573 K, the reaction products may get desorbed immediately after their formation providing the opportunity for new gas species to react with the sensing sites on the film surface [28]. Thus, the LPG reacts most effectively with chemisorbed oxygen at such particular temperature, which results in the significant decrease in the resistance of the film. Therefore, the maximum LPG response of ZnO film is expected at such particular temperature. At higher temperatures (>573 K), the amount of the adsorbed oxygen is less and therefore a lesser amount of ionic species are formed. Therefore, in the presence of LPG, the probability of the reduction reaction of the gas with chemisorbed oxygen is less, which results in a small change in resistance at higher temperatures and decreases the gas response [26,29]. Therefore, the chemically deposited ZnO thin film operates as a sensing element to the LPG only within a specific temperature window. In the present case, the optimum operating temperature for ZnO film is 573 K at which the sensor sensitivity attains its maximum value.

3.5.3. Effect of LPG concentration

The LPG response (*S*%) at various concentrations of LPG is shown in Fig. 9 at an operating temperature of 573 K. The LPG response is increased continuously from 25 to 52% with increasing the gas concentration in the range of 1300–3900 ppm LPG and attained the maximum gas response [30]. At 5200 ppm LPG, it is decreased to 40%. This may be due to the active region of the sensor would be up to 3900 ppm, as the rate of rise of response is larger during this region [31]. At lower gas concentrations (<3900 ppm LPG), the unimolecular layer of gas molecules would be expected to form on the surface, which would interact with the surface more actively giving larger response. There would be multilayer's of gas molecules on the ZnO surface at the higher gas concentrations (>3900 ppm LPG) resulting decrease in gas response [32]. Thus, at 573 K the maximum LPG response of 52% is obtained for mesoporous ZnO upon exposure to 3900 ppm LPG which is higher than reported earlier for ZnO films deposited by CBD method form basic bath [20]. The response and recovery times are also important parameters. Fig. 10 shows the dynamic response transient of mesoporous ZnO sensor upon exposure to 2600 ppm LPG at 573 K. After the removal of LPG, the recovery time is measured till the gas response dropped to the original value. From the plot, the response time of 72 s and corresponding recovery time is 146 s is observed.

3.5.4. Stability study

The long-term stability is another important factor for gas sensors. For the stability study of mesoporous ZnO, repeated experiments are performed at 573 K upon exposure of fixed concentration of 2600 ppm LPG for 60 days with 10 days interval after the first measurement. The variation of LPG response with time is illustrated in Fig. 11. The LPG performance remained almost the same after initial decrease (10%) indicates the mesoporous ZnO sensor can stand as a reliable element for LPG sensor application. The better stability may be resulted due to mesoporous microstructure, such as single crystal structure and morphology maintenance [33].

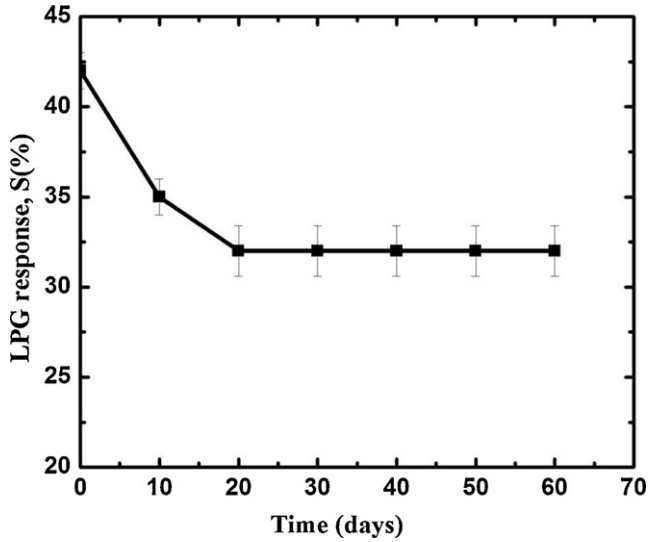

Fig. 11. Stability studies of mesoporous ZnO sensor under the exposure of 2600 ppm LPG at 573 K.

4. Conclusions

In conclusion, an aqueous acidic solution system for growing mesoporous ZnO thin film based LPG sensor from urea containing bath is developed. The present method is simple, inexpensive and easily reproducible. The wurtzite crystal structure of mesoporous ZnO film has been confirmed from the XRD analysis. Hydrophobic surface with contact angle of $128 \pm 1^{\circ}$ and mesoporous morphology having pore size $\sim 2\ \mu m$ has been observed from the SEM. Optical study revealed the presence of direct band with energy 3.24 eV. The LPG sensing performance has been investigated at different operating temperatures and gas concentrations. The mesoporous ZnO thin films exhibits excellent LPG sensing properties with maximum response of 52% upon exposure of 3900 ppm LPG as well as good reproducibility and short response/recovery times because of their mesoporous nature.

Acknowledgement

Authors are grateful to the Department of Science and Technology, New Delhi for financial support through the scheme no. SR/S2/CMP-82/2006. One of the author Dr. D. S. Dhawale greatly thankful to DST for the award of Junior Research Fellowship (JRF).

References

[1] G. Neri, A. Bonavita, G. Rizzo, S. Galvano, N. Pinna, M. Niederberger, S. Capone, P. Siciliano, Sens. Actuators B 122 (2007) 564.
[2] D.S. Dhawale, R.R. Salunkhe, V.J. Fulari, M.C. Rath, N.S. Sawant, C.D. Lokhande, Sens. Actuators B 141 (2009) 58.
[3] V.R. Shinde, T.P. Gujar, C.D. Lokhande, Sens. Actuators B 120 (2007) 551.
[4] R.R. Salunkhe, D.S. Dhawale, D.P. Dubal, C.D. Lokhande, Sens. Actuators B 140 (2009) 86.
[5] J.L. Gunjakar, A.M. More, C.D. Lokhande, Sens. Actuators B 131 (2007) 356.
[6] U. Ozgur, Y.I. Alivov, C. Liu, A. Teke, M.A. Reshchikov, S. Dogan, V. Avrutin, S.J. Cho, H. Morkoc, J. Appl. Phys. 98 (2005) 041301.
[7] D.S. Dhawale, D.P. Dubal, A.M. More, T.P. Gujar, C.D. Lokhande, Sens. Actuators B 147 (2010) 488.
[8] J. Chen, Jin Li, G. Jiahui Li, X. Xiao, J. Yang, J. Alloys Compd. 509 (2011) 740.
[9] A. Forleo, L. Francioso, S. Capone, P. Siciliano, P. Lommens, Z. Hens, Sens. Actuators B 146 (2010) 111.
[10] H.T. Wang, B.S. Kang, F. Ren, L.C. Tien, P.W. Sadik, D.P. Norton, S.J. Pearton, J. Lin, Appl. Phys. Lett. 86 (2005), pp. 243503/1-243503/3.
[11] A.J. Gimenez, J.M.Y. Limon, J.M. Seminari, J. Phys. Chem. C 115 (2011) 282.
[12] Y.X. Du, Q.X. Yuan, J. Alloys Compd. 494 (2010) 468.
[13] C. Gu, J. Huang, Y. Wu, M. Zhai, Y. Sun, J. Liu, J. Alloys Compd. 509 (2011) 4499.
[14] Q.A. Li, H.K. Sun, M. Luo, W.J. Weng, K. Cheng, C.L. Song, P.Y. Du, G. Shen, G.R. Han, J. Alloys Compd. 503 (2010) 514.
[15] F. Xu, Y.N. Lu, L.T. Sun, L.J. Zhi, Chem. Commun. 46 (2010) 3191.
[16] N. Yu, D. Deng, D. Yang, Y. Wang, T. Yang, J. Alloys Compd. 505 (2010) L27.
[17] X.W. Lou, L.A. Archer, Z.C. Yang, Adv. Mater. 20 (2008) 3987.
[18] J.R. Huang, K. Yu, C.P. Gu, M.H. Zhai, Y.J. Wu, M. Yang, J.H. Liu, Sens. Actuators B 147 (2010) 467.
[19] K.P. Stevenson, G.A. Kimmel, Z. Dohnalek, R.S. Smith, B.D. Kay, Science 283 (1999) 1505.
[20] K.V. Gurav, V.J. Fulari, U.M. Patil, C.D. Lokhande, O.S. Joo, Appl. Surf. Sci. 256 (2010) 2680.
[21] S.G. Kandalkar, D.S. Dhawale, C.K. Kim, C.D. Lokhande, Synth. Met. 160 (2010) 1299.
[22] A.A. Sagade, R. Sharma, Sens. Actuators B 133 (2008) 135.
[23] V.R. Shinde, C.D. Lokhande, R.S. Mane, S.H. Han, Appl. Surf. Sci. 245 (2005) 407.
[24] N.J. Dayan, S.R. Sainkar, R.N. Karekar, R.C. Aiyer, Thin Solid Films 325 (1998) 254.
[25] K. Arshak, I. Gaidan, Mater. Sci. Eng. B 118 (2005) 44.
[26] P.P. Sahay, R.K. Nath, Sens. Actuators B 133 (2008) 222.
[27] S. Gupta, R.K. Roy, M. PalChowdhury, A.K. Pal, Vacuum 75 (2004) 111.
[28] T.G. Nenov, S.P. Yordanov, Technomic Publication, Lancaster 1 (1996) 137.
[29] K.A. Ngo, P. Lauque, K. Aguir, Sens. Actuators B 124 (2007) 209.
[30] T.P. Hulser, H. Wiggers, F.E. Kruis, A. Lorke, Sens. Actuators B 109 (2005) 13.
[31] P.P. Sahay, J. Mater. Sci. 40 (2005) 4383.
[32] S.M. Chou, L.G. Teoh, W.H. Lai, Y.H. Su, M.H. Hon, Sensors 6 (2006) 1420.
[33] J. Xu, Y. Zhang, Y. Chen, Q. Xiang, Q. Pan, L. Shi, Mater. Sci. Eng. B 150 (2008) 55.